scientific reports

Check for updates

OPEN

Skeletal muscle mitochondrial dysfunction is associated with increased *Gdf15* expression and circulating GDF15 levels in aged mice

J. Chen[1,4], J. Kastroll[1,4], F. M. Bello[1], M. M. Pangburn[1], A. Murali[1], P. M. Smith[1], K. Rychcik[1], K. E. Loughridge[2], A. M. Vandevender[2], N. Dedousis[1], I. J. Sipula[1], J. K. Alder[2] & M. J. Jurczak[1,3]✉

Growth differentiation factor-15 (GDF15) is a biomarker of multiple disease states and circulating GDF15 levels are increased during aging in both pre-clinical animal models and human studies. Accordingly, multiple stressors have been identified, including mitochondrial dysfunction, that lead to induction of *Gdf15* expression downstream of the integrated stress response (ISR). For some disease states, the source of increased circulating GDF15 is evident based on the specific pathology. Aging, however, presents a less tractable system for understanding the source of increased plasma GDF15 levels in that cellular dysfunction with aging can be pleiotropic and heterogeneous. To better understand which organ or organs contribute to increased circulating GDF15 levels with age, and whether changes in metabolic and mitochondrial dysfunction were associated with these potential changes, we compared young 12-week-old and middle-aged 52-week-old C57BL/6 J mice using a series of metabolic phenotyping studies and by comparing circulating levels of GDF15 and tissue-specific patterns of *Gdf15* expression. Overall, we found that *Gdf15* expression was increased in skeletal muscle but not liver, white or brown adipose tissue, kidney or heart of middle-aged mice, and that insulin sensitivity and mitochondrial respiratory capacity were impaired in middle-aged mice. These data suggest that early changes in skeletal muscle mitochondrial function and metabolism contribute to increased circulating GDF15 levels observed during aging.

Keywords Integrated stress response, Aging, Respirometry, Insulin resistance, Energy expenditure

Growth differentiation factor 15 (GDF15) is a TGF-β superfamily member whose expression in tissues is increased by the integrated stress response (ISR) in response to various stressors[1]. Patients and preclinical models with primary defects in mitochondrial function display increased plasma GDF15 levels[2,3]. Plasma GDF15 levels increase with aging, alongside changes in mitochondrial respiratory capacity, and are associated with loss of lean mass and strength in both patients and animal models[4–6]. At the same time, increased GDF15 is reported to be protective against aging-induced inflammation and metabolic dysfunction in liver[5,7]. Thus, whether elevated plasma GDF15 in the context of aging contributes to or protects against disease remains controversial. A major outstanding question in this area is what cell type or types contribute to increased plasma GDF15 with aging, and whether the site of production affects aging phenotypes.

Similar to observations made in aging, obesity is characterized by an increase in circulating GDF15 levels. Until recently, the tissue-specific origins of increased circulating GDF15 were unclear due to the systemic stress placed on multiple organ systems in obese subjects, including but not limited to liver, skeletal muscle, kidney, adipose tissue and immune cells. We recently published results describing a unique transgenic mouse model

[1]Division of Endocrinology and Metabolism, University of Pittsburgh School of Medicine, 200 Lothrop Street, BST W1060, Pittsburgh, PA 15213, USA. [2]Division of Pulmonary, Allergy and Critical Care Medicine, University of Pittsburgh School of Medicine, Pittsburgh, PA, USA. [3]Center for Metabolism and Mitochondrial Medicine, University of Pittsburgh School of Medicine, Pittsburgh, PA, USA. [4]J. Chen and J. Kastroll are co-first author. ✉email: jurczakm@pitt.edu

where we restored endogenous expression of *Gdf15* specifically in hepatocytes of whole-body *Gdf15* knockout mice, demonstrating that hepatocytes are the primary source of circulating GDF15 during obesity[8]. This conclusion was corroborated independently by a second group using a different genetic approach in mice, as well as samples from human subjects[9], and they further demonstrated that immune cells contribute to these changes but to a lesser degree. The upregulation of *Gdf15* in hepatic and immune cells during obesity is believed to occur downstream of the ISR [2,9–11]. Importantly, activation of the ISR and upregulation of *Gdf15* in the context of liver metabolic disease is reported to occur downstream of ER stress and require ATF4 and CHOP[14–16]. In addition to ER stress, mitochondrial stress, specifically reductive stress in the form of excess NADH, is implicated in activation of the ISR and upregulation of *Gdf15*[2,17]. Given the observation that mitochondrial dysfunction declines with aging and that mitochondrial dysfunction is associated with a loss of metabolic homeostasis and increased *Gdf15* expression, we performed a series of studies in middle-aged mice to determine tissue-specific, aging-dependent changes in insulin sensitivity, mitochondrial function and *Gdf15* expression with the goal of identifying what organs give rise to increased circulating GDF15 during normal aging. We elected to study middle-aged mice (52 weeks or 12 months) as opposed to old mice (18 months or older) based on our experience that metabolic dysfunction occurs early during the aging process prior to other diseases, allowing us to avoid confounding stressors, such as cancer and their effects on GDF15 levels independent of changes in mitochondrial function and metabolism.

Materials and methods

Animal care and use

Male C57BL/6 J mice were purchased from Jackson Labs and housed for eight weeks at the University of Pittsburgh prior to study. Mice were studied at 12 and 52 weeks old. All studies were reviewed and approved by the Institutional Animal Care and Use Committee at the University of Pittsburgh prior to initiation and are consistent with ARRIVE guidelines. All experiments were performed in accordance with the relevant guidelines and regulations. Mice were group housed in a temperature-controlled environment between 20 and 22 °C with 12 h light/12 h dark cycle from 7am to 7 pm with ad libitum access to water and regular chow food (ProLab IsoPro 5P76, catalog #0006972). Mice were individually housed for metabolic cage studies that consisted of 24 h of acclimation followed by 48 h of active data collection using the Promethion Multi-Plexed Metabolic Cage System (Sable Systems). Feeding and running wheel activity are expressed as totals for the light/dark cycles and total time housed in the cages, whereas energy expenditure, calculated by indirect calorimetry using VCO_2 and VO_2, is expressed as the light/dark and 24 h averages. Max sustained speed for running wheel studies was defined as the fastest pace maintained for 10 min during the first two hours of the dark cycle when mice were most engaged with the running wheel and total distances traveled were the greatest. Body composition (fat/lean mass) was measured by EchoMRI. Mice were euthanized after isoflurane anesthesia by cervical dislocation and exsanguination. Mice that underwent hyperinsulinemic euglycemic clamp procedures were euthanized with an intravenous, lethal dose of pentobarbital (150 mg/kg).

Hyperinsulinemic euglycemic clamps

Clamp studies were performed as previously described[24] with minor modifications. Jugular vein catheters were surgically placed five days prior to study. Mice were fasted six hours in the morning prior to a primed/continuous infusion of 3-^{3}H-glucose (Perkin Elmer; prime: 0.7 µCi/kg over 3 min; 0.05 µCi/min basal, 0.1 µCi/min clamp) to measure basal and clamped rates of glucose turnover (whole-body glucose uptake and endogenous or hepatic glucose production). Insulin was given as a primed/continuous infusion (Novolin-R, Novo Nordisk; prime dose: 16 mU/kg over 3 min; continuous dose: 3.0 mU kg^{-1} min^{-1}). Blood was collected by tail vein massage for plasma glucose, tracer and insulin measurements, and a variable infusion of 20% dextrose was administered to maintain euglycemia. Glucose turnover was calculated as the ratio of the 3-[^{3}H]glucose infusion rate to the specific activity of plasma glucose. Endogenous glucose production was calculated as the difference between the glucose infusion rate and the rate of glucose uptake. To determine tissue-specific glucose uptake, a 10-µCi bolus injection of [^{14}C]2-deoxyglucose was given at 90 min. Tissue-specific rates were calculated from the area under the curve of [^{14}C]2-deoxyglucose detected in plasma and the tissue content of [^{14}C]2-deoxyglucose-6-phosphate.

High-resolution respirometry

Liver mitochondrial respiratory capacity was assessed using a mitochondrially enriched liver lysate that was prepared by homogenizing fresh liver in ice-cold mitochondrial isolation buffer, SMET (70 mM sucrose, 220 mM mannitol, 1 mM EDTA and 10 mM Tris–HCl pH 7.4, and 0.25% BSA), using a glass vessel and Teflon pestle. The homogenate was centrifuged at 800 × g for 10 min at 4 °C followed by collection of the supernatant or mitochondrially enriched lysate, which was used for respirometry assays, total protein determination by BCA and citrate synthase activity measure[24]. Skeletal muscle respiratory capacity was measured using permeabilized muscle fiber bundles taken from the soleus. Fibers bundles weighing between 2–3 mg were placed in ice-cold BIOPS buffer (10 mM Ca-EGTA, 0.1 M free calcium, 20 mM imidazole, 20 mM taurine, 50 mM potassium 2-[N-morpholino]-ethanesulfonic acid, 0.5 mM dithiothreitol, 6.56 mM $MgCl_2$, 5.77 mM ATP, and 15 mM phosphocreatinine, pH 7.1) and gently teased apart under a dissecting light microscope, followed by chemical permeabilization with saponin (50 µg/ml in BIOPS) on ice with gentle rocking (25 rpm) for 30 min. Fiber bundles were washed for 10 min twice with ice-cold respiration buffer, MiR05 (0.5 mM EDTA, 3 mM $MgCl_2$-$6H_2O$, 60 mM K-lactobionate, 20 mM taurine, 10 mM KH_2PO_4, 20 mM HEPES, 110 mM sucrose and 0.1% BSA, pH 7.1). Fiber bundle weight was measured after permeabilization using gently dried bundles and an analytical balance. Mitochondrial respiration for liver and skeletal muscle samples was then measured using the Oroboros O_2K platform and MiR05 buffer at 37 °C in a sealed chamber under constant mixing. State 3 and 4 respiration, as well as maximum electron transport chain capacity and non-mitochondrial respiration, were measured using

the following substrate and inhibitor concentrations: pyruvate (5 mM), malate (2 mM) and glutamate (10 mM); adenosine diphosphate (4 mM for liver, titrations of 0.025, 0.2 and 4 mM for soleus); FCCP (0.5 µM titrations to achieve max respiration); Antimycin A (2.5 µM). Respiration that persisted after the addition of antimycin A was subtracted from each of the respiratory states to correct for non-mitochondrial sources of oxygen consumption. The respiratory control ratio (RCR) was calculated as the ratio of state 3 (ADP-stimulated respiration) to state 4 (leak respiration prior to addition of ADP).

Gene expression and biochemical analyses

RNA was extracted from tissue using Trizol and the concentration and purity of the RNA was determined spectrophotometrically. A total of 1 µg RNA was used for cDNA synthesis using Qiagen's QuantiTect Reverse Transcription Kit according to the manufacturer's instructions, including use of a DNAse step prior to synthesis. Gene expression was measured by quantitative PCR using SYBR Green and QuantiTect Primer Assays purchased from Qiagen for *Gdf15, Gadd34, Ddit3,* and *Gapdh*. Gene expression was measured using the Applied Biosystems 7500 Fast Real-Time PCR System. Relative expression was calculated using the measured efficiency of each primer using a four-point standard curve and the Ct-value for the gene of interest and *Gapdh* as the house keeping gene, and then expressed as fold-change relative to the 12-week-old group for the specific gene and tissue. Plasma glucose levels were measured using an Analox GM9 Glucose Analyzer. Plasma insulin and GDF15 levels were measured using ELISA (Crystal Chem, 90,080; R&D Systems, MGD150).

Statistical analyses

Data are reported as the mean ± s.e.m. Comparisons were made using Student's t-test, 2-way ANOVA and ANCOVA where appropriate and noted within the figure legends and $p < 0.05$ was considered significant. ANCOVA was performed to determine the relationship between body weight and energy expenditure using the NIH-funded Mouse Metabolic Phenotyping Center online analysis portal[25].

Results

Energy expenditure, feeding and running wheel activity are reduced in middle-aged C57BL/6 J mice

To establish the relationship between aging, circulating GDF15 levels and associated changes in metabolic homeostasis, we elected to study young, 12-week-old male mice and middle-aged, 52-week-old male mice purchased from Jackson Labs. The 52-week-old mice weighed significantly more than the 12-week-old mice, which was due primarily to increased adiposity (Fig. 1A). The 52-week-old mice weighed approximately 12 g more than the 12-week-old mice, which corresponded to a 3.8 g difference in lean mass and 8.2 g difference in fat mass. Thus, relative lean mass was significantly reduced while fat mass significantly increased in middle-aged compared with young mice (Fig. 1B). Consistent with past reports in old mice[5,26], middle-aged mice demonstrated significantly increased circulating GDF15 levels (Fig. 1C). To understand how aging affected whole-body energy balance and the observed changes in body weight and composition, mice were studied in metabolic cages to measure differences in energy expenditure, feeding and running wheel activity. Due to the differences in adiposity and body weight between groups, we normalized energy expenditure to lean mass and also applied ANCOVA using body weight as a co-variate, which has been recommended as the optimal treatment for such data by multiple groups[27–29]. Energy expenditure normalized to lean mass was significantly reduced in 52-week-old compared with 12-week-old mice during the light cycle, when activity levels are relatively low, as well as the dark cycle and 24 h period average (Fig. 1D, E). ANCOVA analysis using energy expenditure as the response variable and body weight as the co-variate demonstrated a significant reduction in energy expenditure in the older mice (Fig. 1F; $p < 0.01$), which corresponded to a 0.07 kcal/h difference indicated by the change in elevation or y-intercept in Fig. 1F. The ANCOVA-adjusted mean energy expenditure was significantly reduced in 52-week-old compared with 12-week-old mice (0.47 ± 0.02 kcal/h vs. 0.54 ± 0.02 kcal/h; $p < 0.05$). Details of the ANCOVA analysis are included in the data supplement. In addition to reduced energy expenditure, feeding was significantly reduced in 52-week-old mice during the light and dark cycles whether expressed per kg lean mass or on a per mouse (non-normalized) basis (Fig. 1G–I). Lastly, 52-week-old mice demonstrated reduced total distance traveled during volunteer wheel running, as well as max sustained speed (Fig. 1J–L).

Insulin resistance occurs in multiple tissues in middle-aged C57BL/6 J mice

Next, we performed hyperinsulinemic euglycemic clamps with isotope tracers to assess whole-body and tissue-specific insulin sensitivity. There was no difference in basal plasma glucose levels, however, basal insulin levels were significantly increased in 52-week-old mice, suggesting insulin resistance (Fig. 2A and D). Plasma glucose levels were matched at approximately 110 mg/dL during the hyperinsulinemic clamp and the glucose infusion rate required to maintain euglycemia under these conditions was more than two-fold less in 52-week-old mice, indicative of severe whole-body insulin resistance (Fig. 2A, B). Basal rates of endogenous or hepatic glucose production were significantly reduced in the 52-week-old mice, which may explain the lack of basal hyperglycemia (Fig. 2C). Insulin-stimulated rates of hepatic glucose production were significantly increased in 52-week-old compared with 12-week-old mice, indicative of hepatic insulin resistance (Fig. 2C). Indeed, hyperinsulinemia fully suppressed hepatic glucose production in 12-week-old mice (see discussion for interpretation of negative hepatic glucose output) but failed to change the rate of hepatic glucose production in 52-week-old mice. Lastly, clamped plasma insulin levels were significantly increased in 52-week-old mice, even though both groups received the same insulin infusion rate, suggesting impaired insulin clearance by liver (Fig. 2D).

In addition to impaired hepatic insulin sensitivity, 52-week-old mice demonstrated reduced whole-body insulin-stimulated glucose transport (Fig. 3A). To determine which tissues contributed to this whole-body effect, we measured tissue-specific rates of glucose transport using ^{14}C-2-deoxyglucose administered as an

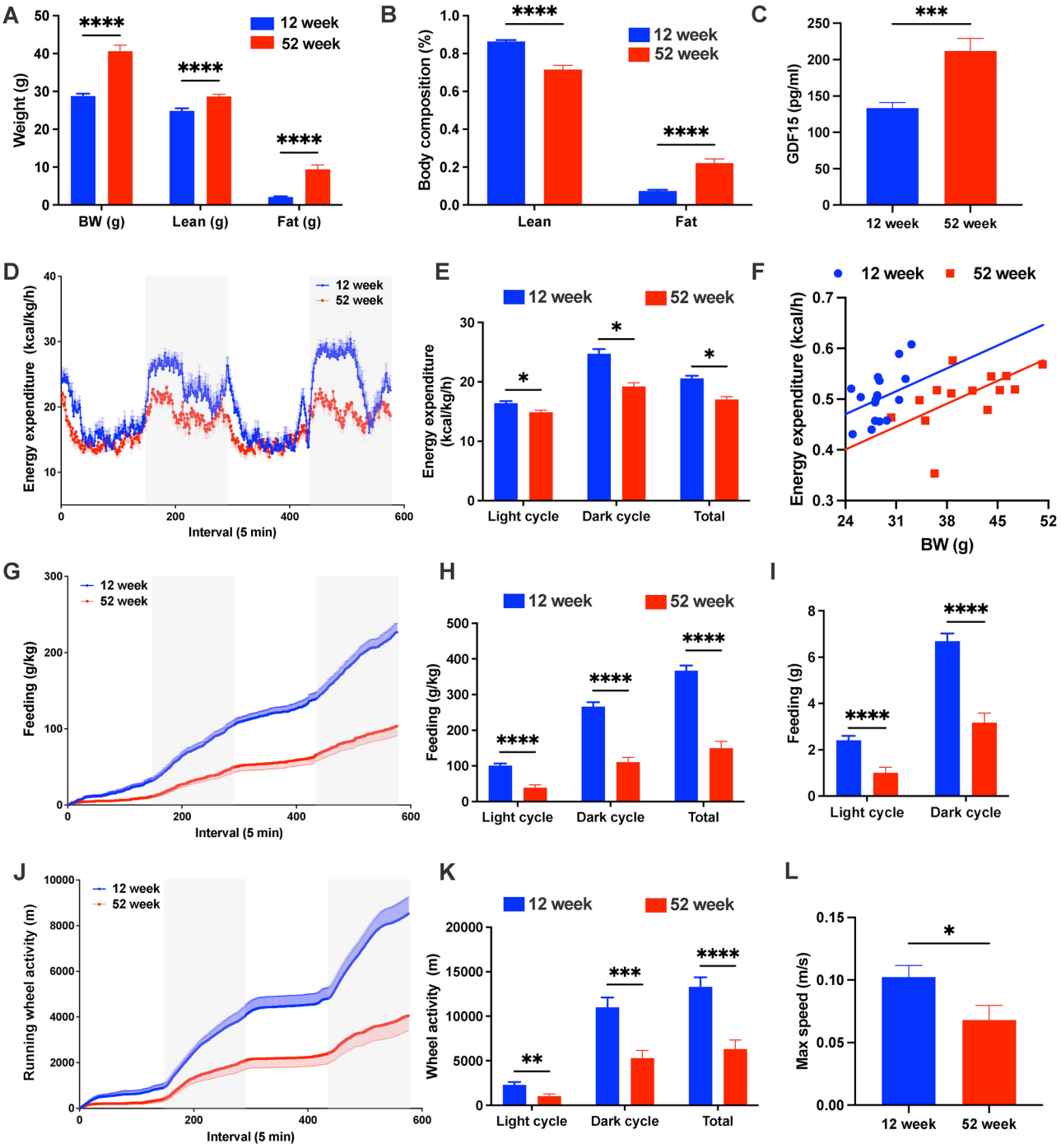

Fig. 1. Energy expenditure, feeding and running wheel activity are reduced and circulating GDF15 levels are increased in middle-aged mice. (**A**) Body weight and composition in grams (**B**) Body composition as a percentage of body weight (**C**) Circulating GDF15 levels. (**D**) Energy expenditure normalized to lean mass over 48 h. E. Light/dark cycle and 24 h average energy expenditure calculated using data in (**D**). (**F**) ANVOCA using energy expenditure as the response variable and body weight as the co-variate. (**G**) Feeding normalized to lean mass over 48 h. (**H**) Light/dark cycle and 48 h total food consumption calculated using data in (**G**). (**I**) Light/dark cycle feeding totals expressed per mouse (non-normalized). (**J**) Running wheel activity in meters traveled over 48 h. (**K**) Light/dark cycle and total distance traveled in running wheel calculated from data in (**J**). (**L**) Max sustained running wheel speed for 10 min interval during first two hours of dark cycle running wheel activity. Data are the mean ± s.e.m. for n = 14–16 mice per group and were analyzed by Student's t-test where $^{*}p < 0.05$, $^{**}p < 0.01$, $^{***}p < 0.001$ and $^{****}p < 0.0001$.

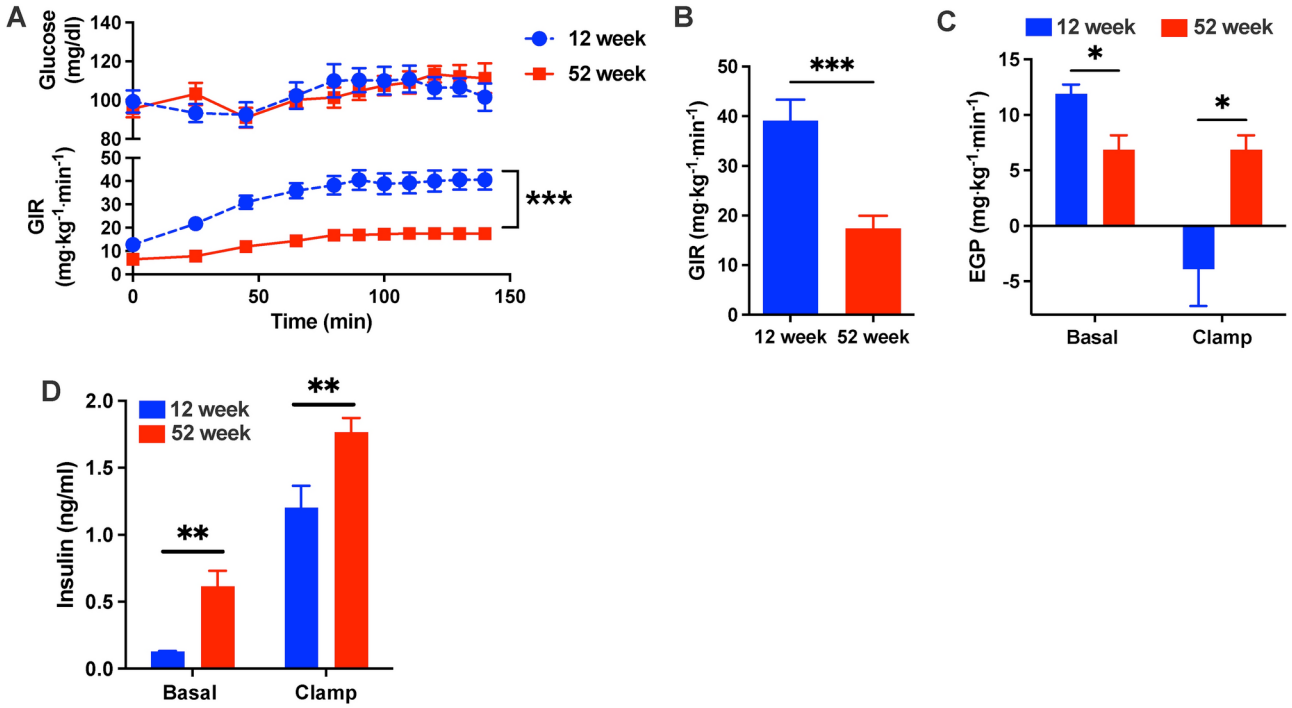

Fig. 2. Whole-body and hepatic insulin sensitivity are impaired in middle-aged mice. (**A**) Plasma glucose levels (upper panel) and the glucose infusion rate (upper panel; GIR) during hyperinsulinemic euglycemic clamp. (**B**) Average GIR during steady-state or the last 40 min of the clamp. (**C**) Rates of endogenous or hepatic glucose production (EGP) in basal (fasted) and clamped (insulin-stimulated) states. (**D**) Basal and clamped plasma insulin levels. Data are the mean ± s.e.m. for n = 6 12-week-old and n = 10 52-week-old mice per group and were analyzed by Student's t-test where $*p < 0.05$, $**p < 0.01$, $***p < 0.001$.

intravenous bolus during the last 50 min of the hyperinsulinemic clamp. Tissue-specific glucose uptake was significantly reduced in skeletal muscle (quadricep), white adipose tissue (gonadal) and brown adipose tissue, while no differences were detected in heart or brain (Fig. 3B–F), although heart trended towards a reduction ($p = 0.07$). Thus, insulin resistance is widespread in middle-aged mice and occurs in liver and peripheral tissues.

Liver and muscle as potential sites of mitochondrial dysfunction and GDF15 production during aging

Hepatic and skeletal muscle mitochondrial dysfunction are associated with insulin resistance[30–33] and mitochondrial stress leads to induction of *Gdf15* expression[2,34,35]. To understand whether the systemic insulin resistance observed in middle-aged mice was associated with mitochondrial dysfunction, as well as to determine which tissues may contribute to increased circulating GDF15 levels in middle-age, we measured *Gdf15* expression in multiple tissues and assessed mitochondrial respiratory capacity in liver and skeletal muscle (soleus). There was a significant 2.5-fold increase in *Gdf15* expression in skeletal muscle (soleus) from 52-week-old mice and no change in liver, kidney, white adipose tissue, brown adipose tissue or kidney (Fig. 4A). *Gdf15* expression is regulated downstream of the integrated stress response (ISR) by the transcription factor DNA damage inducible transcript 3 (*Ddit3*)[15,34], whose expression increases with cellular stress. Consistent with the lack of change in *Gdf15* in liver, *Ddit3* expression was unchanged (Fig. 4B). Growth arrest and DNA damage-inducible protein 34 (*Gadd34*), which is also downstream of the ISR and often co-regulated with *Gdf15* in response to stress[13], was also unchanged in liver of middle-aged mice (Fig. 4B). Despite the presence of hepatic insulin resistance (Fig. 2C), there were no differences in mitochondrial respiratory capacity in 52-week-old compared with 12-week-old mice (Fig. 4C, D). Specifically, state 4 or leak respiration in the presence of pyruvate, malate and glutamate were similar between groups, as were state 3 or oxidative phosphorylation and maximal electron transport chain activity following uncoupling by FCCP (Fig. 4C). Also, the respiratory control ratio or RCR, which serves as a robust integrated readout of mitochondrial function[36], was unchanged in liver (Fig. 4D). Interestingly, citrate synthase activity, which serves as surrogate of mitochondrial content in liver[37], was significantly increased in 52-week-old mice (Fig. 4E), suggesting an increase in mitochondrial mass.

Next, we assessed mitochondrial respiratory capacity using permeabilized muscle fiber bundles from soleus. State 4 or leak respiration was significantly increased in 52-week-old mice (Fig. 5A). State 3 or respiration committed to oxidative phosphorylation was unchanged at both submaximal (0.025–0.2 mM) and maximal (4.0 mM) ADP concentrations (Fig. 5B). Maximum electron transport chain activity in the presence of FCCP was also unchanged in skeletal muscle from 52-week-old mice (Fig. 5C). Accordingly, the RCR at submaximal ADP concentrations was significantly reduced in 52-week-old mice (Fig. 5D), and there was a trend towards

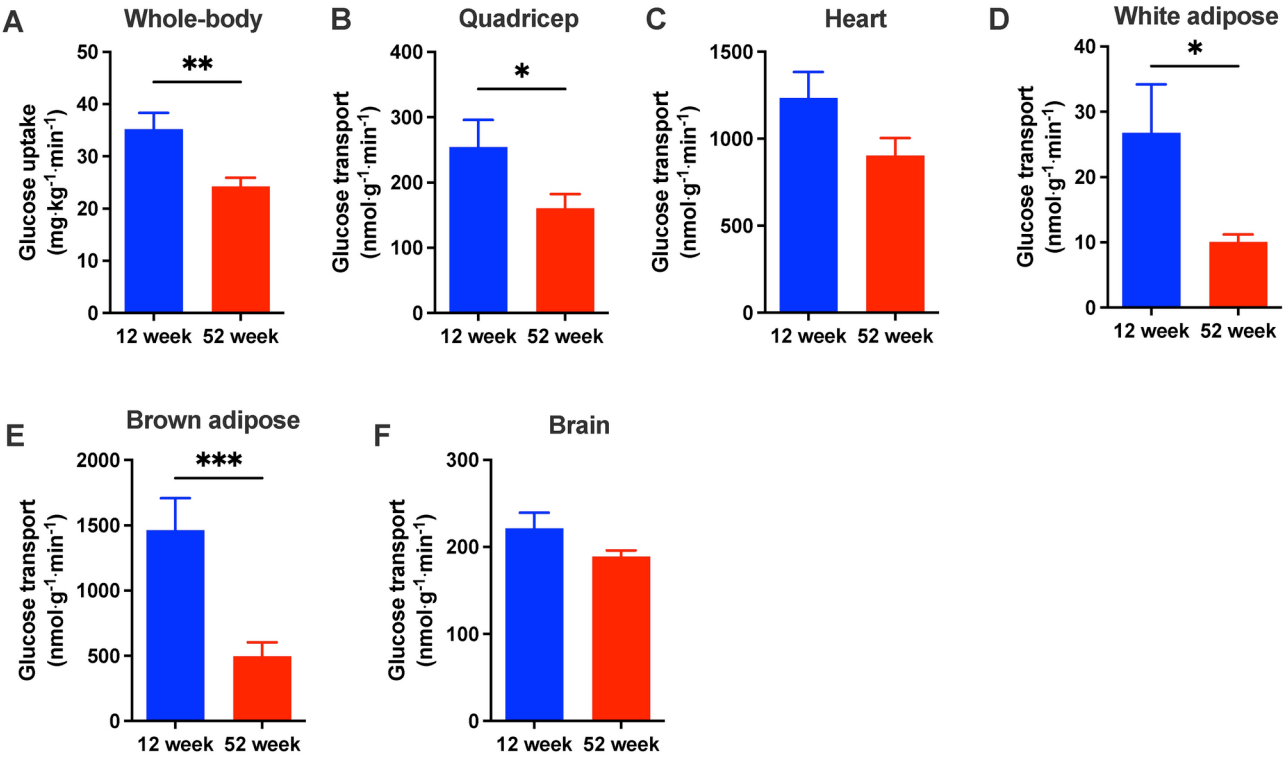

Fig. 3. Whole-body and tissue-specific insulin-stimulated glucose uptake are reduced in middle-aged mice. (**A**) Whole-body glucose uptake during hyperinsulinemic clamp. B-F. Tissue-specific rates of glucose transport measured in skeletal muscle (quadricep) (**B**), heart (**C**), white adipose tissue (**D**), brown adipose tissue (**E**) and brain (**F**). Data are the mean ± s.e.m. for n = 6 for 12-week-old and n = 10 for 52-week-old mice per group and were analyzed by Student's t-test where $^{*}p < 0.05$, $^{**}p < 0.01$, $^{***}p < 0.001$ and $^{****}p < 0.0001$.

reduced RCR at maximal ADP concentration ($p = 0.08$). Consistent with the increase in skeletal muscle *Gdf15* expression, *Ddit3* and *Gadd34* expression were significantly increased 1.9-fold in 52-week-old compared with 12-week-old mice (Fig. 5E), suggesting activation of the ISR in association with mitochondrial dysfunction in middle-aged skeletal muscle.

Discussion

Past studies relating age to changes in circulating GDF15 levels focused primarily on human subjects aged 65 years or older or mouse models aged 18 months or older[4,5,26,26,38]. Here, we elected to study middle-aged 52-week-old mice, corresponding to 38 to 47 year-old humans[39], to understand whether metabolic changes that occur early in the aging process in C57BL/6 J mice were associated with increased circulating GDF15, as well. We found that middle-aged mice were characterized by reduced relative amounts of lean mass and increased fat mass, as well as reduced energy expenditure, running wheel capacity and impaired skeletal muscle mitochondrial function and insulin sensitivity. The insulin resistance and impaired mitochondrial respiratory capacity in skeletal muscle were associated with a 2.5-fold increase in *Gdf15* expression and significantly increased plasma GDF15 levels, suggesting that skeletal muscle is the primary site for increased circulating GDF15 levels observed in middle-aged mice.

Previously, Kim and colleagues examined the relationship between age, skeletal muscle *Gdf15* expression and circulating GDF15 levels in C57BL/6 mice, focusing on 6-, 10-, 14- and 18-month-old mice[26]. They reported a significant effect of age on both *Gdf15* expression and plasma levels but only the 18-month group demonstrated significantly increased expression and circulating levels compared to the 6-month group. In contrast to our work, they did not measure *Gdf15* expression in other tissues, limiting conclusions regarding the source of circulating GDF15. Their results also differed from ours with regards to the observation of increased skeletal muscle *Gdf15* expression and plasma levels in 52-week (12-month) old mice here. This may be due to the fact that we used a younger control group (3 months here vs. 6 months[26]) and may also be due to differences in group sizes (n = 11 here versus n = 4[26]). Regardless of these small differences, they also observed a negative association between GDF15 levels and lean mass, as well skeletal muscle function and endurance capacity, as implied by our running wheel studies. In a second study, Moon and colleagues reported increased hepatic expression of *Gdf15* in association with increased circulating GDF15 when comparing 2- and 20-month-old mice[5]. Using data from the *Tabula Muris Senis*[40], a single-cell transcriptome atlas of tissue from aging mice, they also noted that *Gdf15* was most highly expressed in liver compared with other tissues in 21-month-old mice[5]. Interestingly, within this same analysis, comparison of *Gdf15* expression between 3-month and 12-month-old mice demonstrated

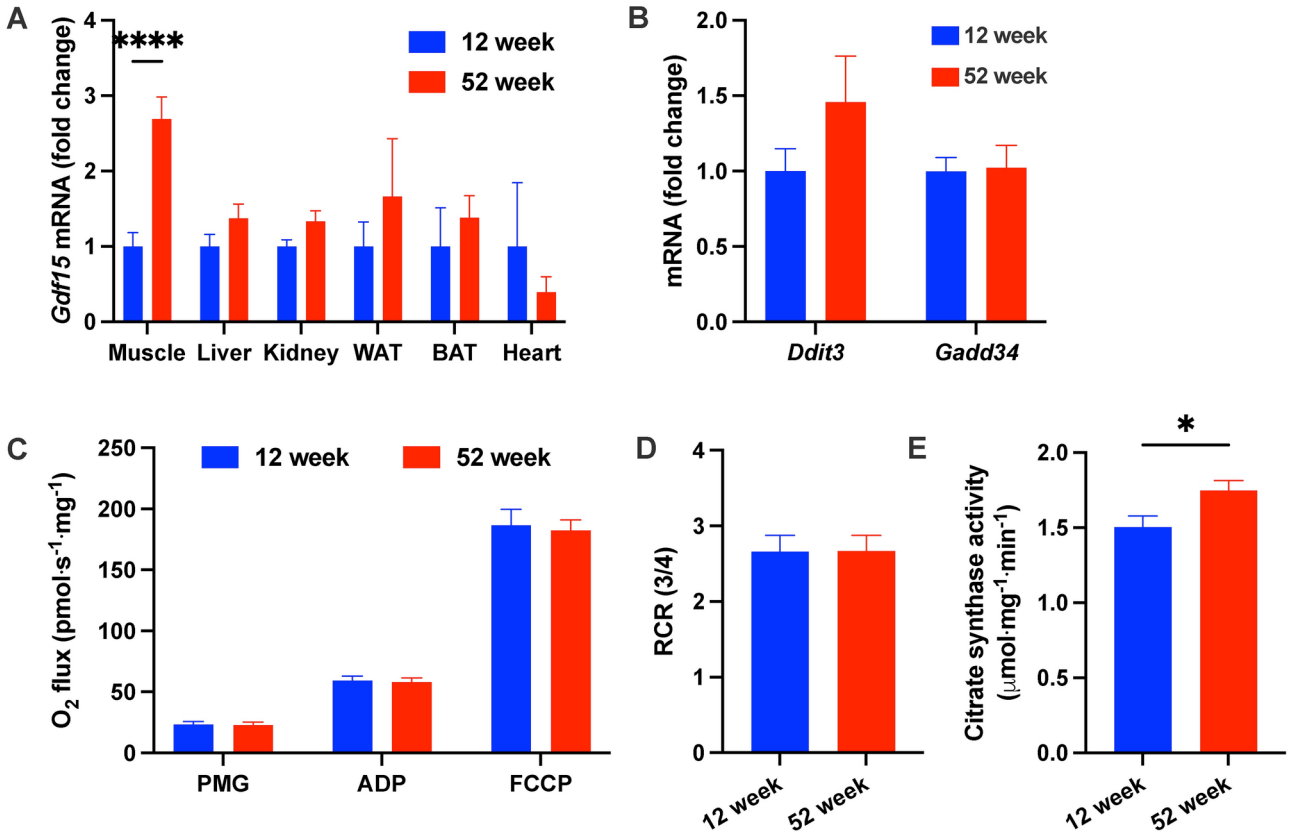

Fig. 4. *Gdf15* expression is increased in skeletal muscle but not other metabolically relevant tissues. (**A**) Quantitative PCR for *Gdf15* mRNA using *Gapdh* as a reference gene and expressed as fold-change relative to 12-week samples for each tissue. (**B**) Liver *Ddit3* and *Gadd34* expression measured by quantitative PCR using *Gapdh* as a reference gene and expressed as fold change relative to 12-week-old mice. (**C**) Mitochondrial respiratory capacity measured from liver samples in the presence of pyruvate, malate and glutamate (PMG; state 4), 4 mM ADP (state 3) and during uncoupling (FCCP). (**D**) Respiratory control ratio (RCR) calculated from data in C. (**E**) Citrate synthase activity measured from mitochondrially enriched liver lysates used in C. Data are the mean ± s.e.m. for n = 11 per group and were analyzed by Student's t-test where $^{*}p < 0.05$.

no difference in liver *Gdf15* expression, similar to observations here. Thus, our data alongside reports in the literature suggest that skeletal muscle is the primary contributor to increased circulating GDF15 levels seen with middle-age and that liver takes on a more important role as aging progresses. These observations also suggest that the underlying stress signals for *Gdf15* induction, whether due to mitochondrial dysfunction or insulin resistance, occur earlier in skeletal muscle than liver.

Studies addressing the relationship between aging and insulin resistance in humans are often difficult to interpret due to differences in body weight and fat and lean mass in elderly compared with young subjects, resulting in some studies reporting increased insulin resistance with aging while others do not[41,42]. In a study where body weight was matched between young and older subjects and insulin resistance was assessed using the 'gold standard' hyperinsulinemic euglycemic clamp, insulin sensitivity was impaired specifically in skeletal muscle in the aged group in association with reduced mitochondrial ATP synthetic capacity, assessed in vivo by ^{31}P-NMR[31]. Similar results have been reported in mouse models where insulin resistance in aged mice (16-months) is present in skeletal muscle and liver[43], similar to our findings here in middle-aged mice. Our data demonstrate that insulin resistance is an early feature of aging that occurs as early as middle age (12 months) in mice. Furthermore, insulin resistance in skeletal muscle was associated with mitochondrial dysfunction, similar to what is observed in humans[31], whereas insulin resistance in liver was associated with intact mitochondrial respiratory capacity but an increase in mitochondrial mass, potentially masking mitochondrial dysfunction.

A relationship between skeletal muscle mitochondrial dysfunction and insulin resistance has been described for both patients with type 2 diabetes and in elderly subjects[31,44–47]. In patients with type 2 diabetes, mitochondrial dysfunction was attributed to both reduced mitochondrial content in muscle[46], as well as impaired electron transport chain capacity during state 3 respiration and uncoupled respiration, independent of changes in mitochondrial content[44,45]. In elderly subjects with insulin resistance, skeletal muscle mitochondrial oxidative capacity was reduced compared with young controls when assessed in vivo, suggesting the potential for either reduced content or function or both[31]. More recently, a multi-center study where 879 older adults were recruited for assessment of skeletal muscle mitochondrial function and metrics of dysmotility reported that older adults with diabetes had reduced maximal electron transport chain capacity compared to older adults without diabetes[47].

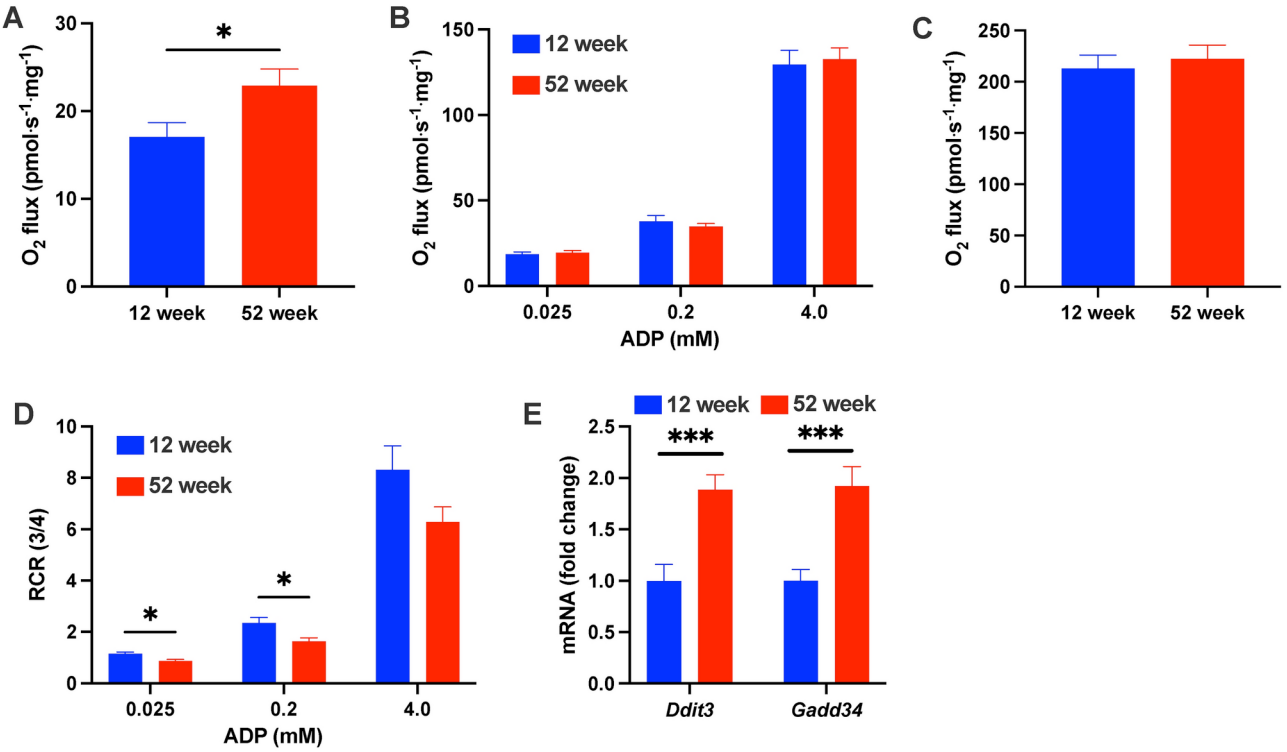

Fig. 5. Mitochondrial respiratory capacity is impaired in middle-aged mice in association with increased expression of markers of the integrated stress response. (**A**) State 4 or leak respiration measured from permeabilized muscle fiber bundles from soleus in the presence of pyruvate, malate and glutamate. (**B**) State 3 respiration measured in the presence of submaximal (0.025–0.20 mM) and maximal (4.0 mM) ADP. (**C**) Maximum electron transport chain capacity measured following uncoupling by FCCP titration. (**B**). Respiratory control ratio (RCR) calculated from data in B. (**E**) Skeletal muscle *Ddit3* and *Gadd34* expression measured by quantitative PCR using *Gapdh* as a reference gene and expressed as fold change relative to 12-week-old mice. Data are the mean ± s.e.m. for n = 11 per group and were analyzed by Student's t-test where $^{*}p < 0.05$.

Another more recent study exploring the relationship between aging and skeletal muscle mitochondrial function reported impaired mitochondrial ADP sensitivity in aged subjects, despite no change in respiratory capacity, and an increase in the fraction of electron leak to reactive oxygen species (ROS) production across a range of ADP concentrations[48]. Although not directly comparable to our results due to differences in methodology, our observation of increased leak respiration and impaired RCR at submaximal ADP concentrations, despite no change in respiratory capacity, suggests similar effects on ADP sensitivity and ROS production in skeletal muscle of middle-aged mice. The authors of this study speculated that redox-induced inhibition of the adenine nucleotide translocase (ANT) may cause the impaired ADP sensitivity in aged skeletal muscle, which may contribute to our observed changes, as well. Future studies measuring H_2O_2 production alongside respiration during ADP titrations or in combination with the creatine kinase clamp approach[49] are warranted, as are ANT protein abundances and redox-dependent modifications at susceptible amino acid residues.

In summary, our study expands upon past work linking aging and mitochondrial dysfunction to increased levels of circulating GDF15 by demonstrating that metabolic dysfunction occurs early in middle-aged mice and is associated with impaired mitochondrial function and upregulation of *Gdf15* expression specifically in skeletal muscle and not liver, heart, kidney, or white and brown adipose tissue. Our studies are limited by several factors. First, for technical reasons, skeletal muscles with different fiber type compositions were used for assessing in vivo insulin-stimulated glucose transport (quadricep) and ex vivo mitochondrial function and *Gdf15* expression (soleus), such that associations drawn between these endpoints should be interpreted with caution. Also, the observations made throughout these studies are associative in nature and future work using genetic approaches to modulate mitochondrial function and *Gdf15* expression in a tissue-specific fashion to firmly establish the relationships identified here will be necessary.

Data availability

Data and resources presented here will be made readily available upon request to the corresponding author.

Received: 26 September 2024; Accepted: 28 February 2025
Published online: 08 March 2025

References

1. Lockhart, S. M., Saudek, V. & O'Rahilly, S. GDF15: A hormone conveying somatic distress to the brain. *Endocr. Rev.* **41**, bnaa007 (2020).
2. Sharma, R. et al. Circulating markers of NADH-reductive stress correlate with mitochondrial disease severity. *J. Clin. Invest.* **131**, e136055 (2021).
3. Ost, M. et al. Muscle-derived GDF15 drives diurnal anorexia and systemic metabolic remodeling during mitochondrial stress. *EMBO Rep.* **21**, e48804 (2020).
4. Liu, H. et al. GDF15 as a biomarker of ageing. *Exp. Gerontol.* **146**, 111228 (2021).
5. Moon, J. S. et al. Growth differentiation factor 15 protects against the aging-mediated systemic inflammatory response in humans and mice. *Aging Cell* **19**, e13195 (2020).
6. Nishikawa, R. et al. Association between serum GDF-15, myostatin, and sarcopenia in cardiovascular surgery patients. *Int. J. Cardiol. Heart Vasc.* **42**, 101114 (2022).
7. Chung, H. K. et al. GDF15 deficiency exacerbates chronic alcohol- and carbon tetrachloride-induced liver injury. *Sci. Rep.* **7**, 17238 (2017).
8. Xie, B. et al. Hepatocyte-derived GDF15 suppresses feeding and improves insulin sensitivity in obese mice. *iScience* **25**, 105569 (2022).
9. Patel, S. et al. Combined genetic deletion of GDF15 and FGF21 has modest effects on body weight, hepatic steatosis and insulin resistance in high fat fed mice. *Mol. Metab.* **65**, 101589 (2022).
10. Kim, K. H. & Lee, M.-S. GDF15 as a central mediator for integrated stress response and a promising therapeutic molecule for metabolic disorders and NASH. *Biochim. Biophys. Acta BBA Gen. Subj.* **1865**, 129834 (2021).
11. Wang, D. et al. GDF15: Emerging biology and therapeutic applications for obesity and cardiometabolic disease. *Nat. Rev. Endocrinol.* **17**, 592–607 (2021).
12 Costa-Mattioli, M. & Walter, P. The integrated stress response: From mechanism to disease. *Science* **368**, eaat5314 (2020).
13. Pakos-Zebrucka, K. et al. The integrated stress response. *EMBO Rep.* **17**, 1374–1395 (2016).
14. Kim, K. H. et al. Growth differentiation factor 15 ameliorates nonalcoholic steatohepatitis and related metabolic disorders in mice. *Sci. Rep.* **8**, 6789 (2018).
15. Li, D., Zhang, H. & Zhong, Y. Hepatic GDF15 is regulated by CHOP of the unfolded protein response and alleviates NAFLD progression in obese mice. *Biochem. Biophys. Res. Commun.* **498**, 388–394 (2018).
16. Patel, S. et al. GDF15 provides an endocrine signal of nutritional stress in mice and humans. *Cell Metab.* **29**, 707-718.e8 (2019).
17 Mick, E. et al. Distinct mitochondrial defects trigger the integrated stress response depending on the metabolic state of the cell. *eLife* **9**, e49178 (2020).
18. Goodman, R. P. et al. Hepatic NADH reductive stress underlies common variation in metabolic traits. *Nature* **583**, 122–126 (2020).
19. Cobb, J. et al. α-Hydroxybutyric acid is a selective metabolite biomarker of impaired glucose tolerance. *Diabetes Care* **39**, 988–995 (2016).
20. Gall, W. E. et al. alpha-hydroxybutyrate is an early biomarker of insulin resistance and glucose intolerance in a nondiabetic population. *PloS One* **5**, e10883 (2010).
21. Thompson Legault, J. et al. A metabolic signature of mitochondrial dysfunction revealed through a monogenic form of leigh syndrome. *Cell Rep.* **13**, 981–989 (2015).
22. Madiraju, A. K. et al. Metformin suppresses gluconeogenesis by inhibiting mitochondrial glycerophosphate dehydrogenase. *Nature* **510**, 542–546 (2014).
23. Day, E. A. et al. Metformin-induced increases in GDF15 are important for suppressing appetite and promoting weight loss. *Nat. Metab.* **1**, 1202–1208 (2019).
24. Edmunds, L. R. et al. Liver-specific Prkn knockout mice are more susceptible to diet-induced hepatic steatosis and insulin resistance. *Mol. Metab.* **41**, 101051 (2020).
25. MMPC: MMPC Energy Expenditure Analysis Page. https://www.mmpc.org/shared/regression.aspx.
26. Kim, H., Kim, K. M., Kang, M. J. & Lim, S. Growth differentiation factor-15 as a biomarker for sarcopenia in aging humans and mice. *Exp. Gerontol.* **142**, 111115 (2020).
27. Arch, J. R. S., Hislop, D., Wang, S. J. Y. & Speakman, J. R. Some mathematical and technical issues in the measurement and interpretation of open-circuit indirect calorimetry in small animals. *Int. J. Obes.* **30**, 1322–1331 (2006).
28. Kaiyala, K. J. & Schwartz, M. W. Toward a more complete (and less controversial) understanding of energy expenditure and its role in obesity pathogenesis. *Diabetes* **60**, 17–23 (2011).
29. Tschöp, M. H. et al. A guide to analysis of mouse energy metabolism. *Nat. Methods* **9**, 57–63 (2012).
30. Petersen, K. F., Dufour, S., Befroy, D., Garcia, R. & Shulman, G. I. Impaired mitochondrial activity in the insulin-resistant offspring of patients with type 2 diabetes. *N. Engl. J. Med.* **350**, 664–671 (2004).
31. Petersen, K. F. et al. Mitochondrial dysfunction in the elderly: possible role in insulin resistance. *Science* **300**, 1140–1142 (2003).
32. Sunny, N. E., Parks, E. J., Browning, J. D. & Burgess, S. C. Excessive hepatic mitochondrial TCA cycle and gluconeogenesis in humans with nonalcoholic fatty liver disease. *Cell Metab.* **14**, 804–810 (2011).
33. Satapati, S. et al. Mitochondrial metabolism mediates oxidative stress and inflammation in fatty liver. *J. Clin. Invest.* **125**, 4447–4462 (2015).
34 Mick, E. et al. Distinct mitochondrial defects trigger the integrated stress response depending on the metabolic state of the cell. *eLife* **9**, e49178 (2020).
35. Davis, R. L., Liang, C. & Sue, C. M. A comparison of current serum biomarkers as diagnostic indicators of mitochondrial diseases. *Neurology* **86**, 2010–2015 (2016).
36. Brand, M. D. & Nicholls, D. G. Assessing mitochondrial dysfunction in cells. *Biochem. J.* **435**, 297–312 (2011).
37. McLaughlin, K. L. et al. Novel approach to quantify mitochondrial content and intrinsic bioenergetic efficiency across organs. *Sci. Rep.* **10**, 17599 (2020).
38. Arauna, D. et al. Older adults with frailty syndrome present an altered platelet function and an increased level of circulating oxidative stress and mitochondrial dysfunction biomarker GDF-15. *Free Radic. Biol. Med.* **149**, 64–71 (2020).
39. When are mice considered old? *The Jackson Laboratory* https://www.jax.org/news-and-insights/jax-blog/2017/november/when-are-mice-considered-old.
40. Almanzar, N. et al. A single-cell transcriptomic atlas characterizes ageing tissues in the mouse. *Nature* **583**, 590–595 (2020).
41. Basu, R. et al. Mechanisms of the age-associated deterioration in glucose tolerance: Contribution of alterations in insulin secretion, action, and clearance. *Diabetes* **52**, 1738–1748 (2003).
42. Ehrhardt, N. et al. Adiposity-independent effects of aging on insulin sensitivity and clearance in mice and humans. *Obes. Silver Spring Md* **27**, 434–443 (2019).
43. González-Rodríguez, A. et al. Essential role of protein tyrosine phosphatase 1B in obesity-induced inflammation and peripheral insulin resistance during aging. *Aging Cell* **11**, 284–296 (2012).
44. Mogensen, M. et al. Mitochondrial respiration is decreased in skeletal muscle of patients with type 2 diabetes. *Diabetes* **56**, 1592–1599 (2007).
45. Phielix, E. et al. Lower intrinsic ADP-stimulated mitochondrial respiration underlies in vivo mitochondrial dysfunction in muscle of male type 2 diabetic patients. *Diabetes* **57**, 2943–2949 (2008).

46. Kelley, D. E., He, J., Menshikova, E. V. & Ritov, V. B. Dysfunction of mitochondria in human skeletal muscle in type 2 diabetes. *Diabetes* **51**, 2944–2950 (2002).
47. Ramos, S. V. et al. Role of cardiorespiratory fitness and mitochondrial oxidative capacity in reduced walk speed of older adults with diabetes. *Diabetes* **73**, 1048–1057 (2024).
48. Holloway, G. P. et al. Age-associated impairments in mitochondrial ADP sensitivity contribute to redox stress in senescent human skeletal muscle. *Cell Rep.* **22**, 2837–2848 (2018).
49. Fisher-Wellman, K. H. et al. Mitochondrial diagnostics: A multiplexed assay platform for comprehensive assessment of mitochondrial energy fluxes. *Cell Rep.* **24**, 3593-3606.e10 (2018).

Acknowledgements
This work was supported by funding from the NIH (R01 DK114012 to M.J.J., T32 DK007052 to A.M.).

Author contributions
M.J.J. and J.C. conceived the study. J.C., J.K., F.M.B, M.M.P., A.M., P.M.S., K.R., K.E.L., A.M.V., N.D., and I.S. and performed experiments. J.C., J.K., F.M.B., I.S., J.K.A. and M.J.J. developed methods, analyzed data and interpreted results. J.C., J.K. and M.J.J. designed and planned the experiments. J.C., J.K., J.K.A. and M.J.J. wrote edited the manuscript. All authors contributed to the preparation of manuscript and approved the final version.

Funding
National Institute of Diabetes and Digestive and Kidney Diseases, DK114012.

Declarations

Competing interests
The authors declare no competing interests.

Additional information
Supplementary Information The online version contains supplementary material available at https://doi.org/10.1038/s41598-025-92572-x.

Correspondence and requests for materials should be addressed to M.J.J.